JOURNAL OF SOLID STATE CHEMISTRY 71, 139–153 (1987)

# Multiple Empty Tunnels in a New Ta–P–S Phase: Synthesis and Structure Determination of $Ta_2P_2S_{11}$

M. EVAIN, S. LEE,* M. QUEIGNEC, AND R. BREC†

*Laboratoire de Chimie des Solides, Faculté des Sciences, 2, rue de la Houssinière, 44072 Nantes Cédex, France*

Received October 30, 1986

$Ta_2P_2S_{11}$ is a new phase of the Ta–P–S system obtained by high-temperature synthesis from the elements. Single-crystal diffraction analysis showed the phase to crystallize in the $P2_1/c$ space group with the following cell parameters: $a = 6.876(3)$ Å, $b = 24.109(8)$ Å, $c = 26.411(8)$ Å, $\beta = 106.04(3)°$, $V = 4208(6)$ Å$^3$, and $Z = 10$. Low-temperature ($T = 140$ K) structure study has been performed and 3104 independent diffractometer data have been refined, with 328 variables, to $R = 8.9\%$. The structure is made of two types of polyhedra, a tetrahedral group ($PS_4$) (mean $d_{P-S} = 2.030$ Å) and a bipolyhedral group ($Ta_2S_{11}$) (mean $d_{Ta-S} = 2.494$ Å) in which tantalum is heptacoordinated. These ($Ta_2S_{11}$) units are formed of two distorted ($TaS_7$) groups sharing a triangular face made of mono- and disulfide anions ($(S_2)^{-II}$–$S^{-II}$). Of the three kinds of ($Ta_2S_{11}$) bipolyhedra, two of them show disorder of the common triangular sulfur face. The way the coordination groups are bonded to one another determines the occurrence of three kinds of tunnels in the structure. Their characteristics and the reason of their emptiness are related to their size and to the special linking arrangement taking place between the ($PS_4$) and ($Ta_2S_{11}$) groups. With the formulation $Ta_2^{V}P_2^{V}(S_2)^{-II}(S^{-II})_9$ the phase is expected to be diamagnetic and semiconducting or insulator. 

## 1. Introduction

Low-dimensional $M$–P–S phases may occur for high sulfur content and for small electronegativity differences between $M$ and S atoms. These conditions ensure that the cation will share oriented bonds mostly with surrounding anions of its coordination group (octahedron, tetrahedron, trigonal prism, trigonal antiprism, etc.) and that the charge borne by the chalcogen ion will be very small. Combinations of the coordination groups through edge, face, or corner sharing allow them to constitute chains or sheets that can be stacked upon one another because of the very low repulsion between weakly charged anions, thus building stable one- or two-dimensional phases. In the $M$–P–S family, $M$ being a VD metal, this is conveniently illustrated by the vanadium derivatives that present only 1-D and 2-D structures for the sulfur-rich materials (Table I). Although it is more electropositive, niobium maintains, in its Nb–P–S phases, mostly low-dimensional structures. However, no 1-D arrangements are found and the phase $NbP_2S_8$ presents both 2-D and 3-D structures. To date, tantalum derivatives, Ta–P–S, constitute exclusively tridimensional arrays, with increased electropositivity (Table I). Niobium is thus, in that group of compounds, a frontier element separating more covalent 1-D and 2-D

* NATO postdoctoral fellow.

† To whom correspondence should be addressed.



0022-4596/87 $3.00

TABLE I

VD TRANSITION METALS THIOPHOSPHATES AND THEIR DIMENSIONALITY

| Vanadium | | | Niobium | | | Tantalum | | |
|---|---|---|---|---|---|---|---|---|
| (2-D) | $V_{0.78}PS_3$ | (1) | (2-D) | $Nb_2PS_{10}$ | (5) | (3-D) | $TaPS_6$ | (9) |
| (2-D) | $P_{0.2}VS_2$ | (2) | (2-D) | $Nb_4P_2S_{21}$ | (6) | (3-D) | $Ta_4P_4S_{29}$ | (10) |
| (1-D) | $V_2PS_{10}$ | (3) | (2-D) | $NbP_2S_8$ | (7) | (3-D) | $TaPS_6Se$ | (11) |
| (2-D) | $V_2P_4S_{13}$ | (4) | (3-D) | $NbP_2S_8$ | (8) | (3-D) | $Ta_2P_2S_{11}$ | |

*Note.* Niobium represents a frontier element between vanadium that gives only low-dimensional (1-D) and (2-D) derivatives and tantalum that leads exclusively to three-dimensional crystal networks.

vanadium derivatives from more ionic 3-D tantalum phases. Among these latter, the two phases, $TaPS_6$ and $Ta_4P_4S_{29}$, constitute attractive materials with tunnels in their atomic arrays (*8*, *9*). It was tempting to further investigate the Ta–P–S system to find new compounds and to verify whether the tunnel structures would again occur. This is the case for the new phase $Ta_2P_2S_{11}$ for which synthesis and structure determinations are reported in this paper.

## 2. Experimental

Small amounts of $Ta_2P_2S_{11}$ crystals were obtained, in evacuated silica tubes, by heating the elements in the Ta/P/S ratio 4/5/24 at 600°C for about 10 days. Attempts to prepare the phase from the stoichiometric proportions resulted in samples containing mostly the $TaPS_6$ phase, the composition of which is very close to that of the compound studied. Microprobe analysis (microsonde Ouest Ifremer) was difficult to perform because of the instability of the phase under the electron beam and/or of the poor crystal surface quality. The best analytical run reported (Table II) is, however, in satisfactory agreement with the $Ta_2P_2S_{11}$ formula, which was also obtained from the structural determination. Only the convergence of analytical and structural data could ascertain the phase stoichiometry, since many other formulas could be imagined in relation to the complex charge balance taking place through various oxidation states of the anions in these types of phases.

The samples of $Ta_2P_2S_{11}$ are elongated parallelepipedic crystals. As can be seen in Fig. 1, the needles are hollow and constituted of many smaller crystals. This corresponds to heavy twinning that was systematically observed in diffraction patterns. After numerous attempts, breaking the crystal edges and/or corners yielded tiny untwinned samples. The X-ray diffraction pattern indicated rather weak intensities and not very sharp spots. The symmetry

TABLE II

ANALYTICAL AND CRYSTALLOGRAPHIC DATA: PARAMETERS OF THE X-RAY DATA COLLECTION AND REFINEMENT

Physical, crystallographic, and analytical data
Formula: $Ta_2P_2S_{11}$ Molecular weight: 776.54 g
Theoretical weight fraction concentration:
Ta: 46.6%, P: 8.0%, S: 45.3%
Microprobe analysis:
Ta: 43.6%, P: 8.3%, S: 45.3%
Crystal symmetry: Monoclinic Space group: $P2_1/c$
Cell parameters (293 K):
$a$ = 6.876(3) Å, $b$ = 24.109(8) Å, $c$ = 26.411(8), Å,
$\beta$ = 106.04(3)°, $V$ = 4208(6) Å$^3$, $Z$ = 10
Cell parameters (140 K):
$a$ = 6.84(1) Å, $b$ = 24.058(9) Å, $c$ = 26.34(3) Å,
$\beta$ = 105.80(8)°, $V$ = 4171(14) Å$^3$
Density: $\rho_{cal}$ = 3.062
Absorption factor: $\mu$(λMo$K\alpha$): 144.5 cm$^{-1}$
Crystal size: ≈0.10 × 0.10 × 0.07 mm$^3$

Data collection
Temperature: 140 K Radiation: Mo$K\alpha$
Monochromator: oriented graphite (002) Scan mode: $\omega/2\,\theta$
Recording angle range: 1–23° Scan angle: 1.00 + 0.35 tan $\theta$
Values determining the scan speed:
SIGPRE: 0.85, SIGMA: 0.01, VPRE: 20 min$^{-1}$,
TMAX = 60 sec
Standard reflection: 0 9 $\bar{2}$, 0 3 1 Periodicity: 3600 sec

Refinement conditions
Reflections for the refinement of the cell dimensions: 25
Recorded reflections in the quarter-space: 6558
Utilized reflections: 3104 with $I > 3\,\sigma(I)$
Refined parameters: 328
Reliability factors: $R = \Sigma||F_o| - |F_c||/\Sigma|F_o|$
$R_w = [\Sigma w(|F_o| - |F_c|)^2/\Sigma wF_o^2/\Sigma wF_o^2]^{1/2}$

Refinement results
$R$ = 8.9% $R_w$ = 11.4%
Extinction coefficient: $E_c$ = 1.3(4) × 10$^{-8}$
Difference Fourier maximum peak intensity: 3.1(6) $e^-$/Å$^3$

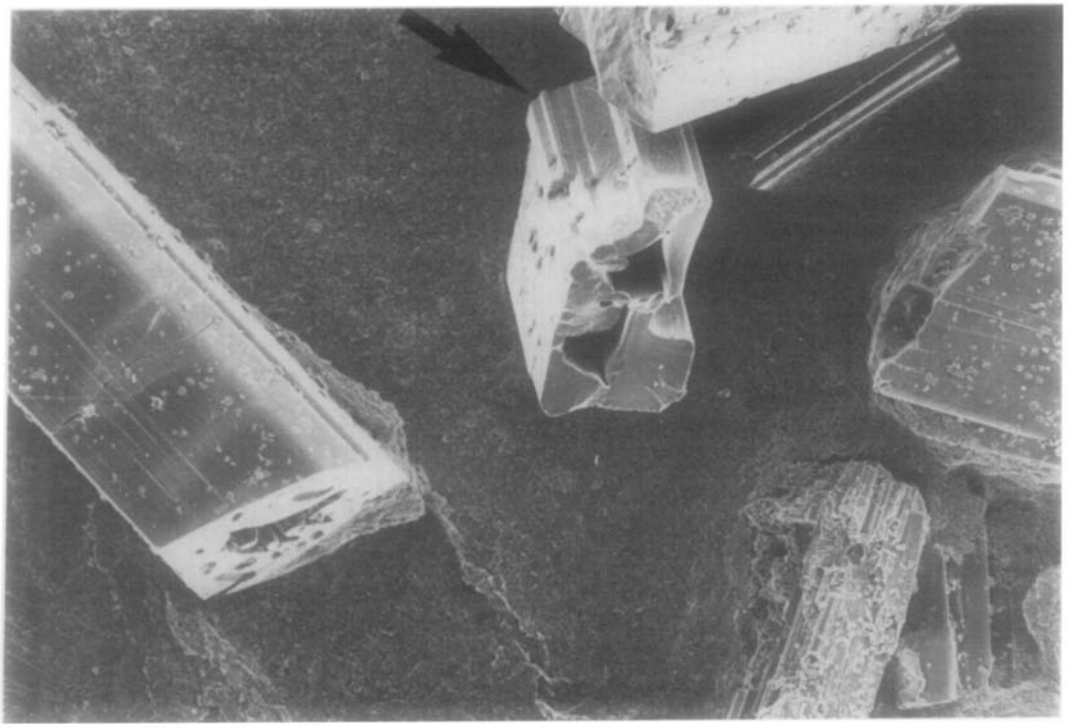

FIG. 1. Photograph showing the curious hollow feature of the $Ta_2P_2S_{11}$ crystals (×75). Arrow indicates a heavy twinning region.

was found to be monoclinic with $P2_1/c$ space group.

Intensity recording on a CAD4 diffractometer with a cathode power set at 1 kW showed, on three different runs, a fast, steady decrease of the standard intensities, attributed to the compound's instability under the X-ray beam and/or to reaction with air. Samples were then sealed into capillaries, the X-ray tube power was lowered to 800 W, and recording of data was resumed. Stability of the standard reflection intensities became then satisfactory and an independent space was recorded. Subsequent structure refinement yielded coherent structural features with very high thermal factors for the atoms, however, and unacceptable low sulfur–sulfur distances in some $S_2$ pairs. Observation of low-temperature $Ta_2P_2S_{11}$ electronic diffraction patterns revealed very sharp diffraction spots and it was decided to record the X-ray diffraction spectrum intensities at low temperature (140 K), in the hope of obtaining better contrasted reflection peaks and a better resolved structure. From this new set of data, the structure refinement carried out using previous atomic positions gave lower thermal vibrations and more homogeneous and better interatomic distances. It is, hence, these results that are reported here. Because the crystal had ill-formed faces, the intensities were not corrected for absorption. The SDP-PLUS program chain (1982 version) of Enraf–Nonius, written by Frenz (*12*), was used to solve the structure. Table II presents the analytical and crystallographic data and parameters of the X-ray data collection and refinement. The room temperature cell parameters were obtained

TABLE III

$Ta_2P_2S_{11}$ X-RAY POWDER DIFFRACTION DATA

| $d_{obs}$(Å) | $d_{calc}$(Å) | $hkl$ | $100 \times I/I_0$ | $d_{obs}$(Å) | $d_{calc}$(Å) | $hkl$ | $100 \times I/I_0$ |
|---|---|---|---|---|---|---|---|
| 8.75 | 8.74 | 022 | 69 | 3.336 | 3.332 | $20\bar{4}$ | 6 |
| 8.00 | 7.98 | 013 | 100 | | 3.338 | 153 | |
| 7.67 | 7.66 | 031 | 88 | 3.302 | 3.305 | $03\bar{7}$ | 2 |
| 6.94 | 6.93 | 023 | 39 | | 3.308 | $13\bar{7}$ | |
| 6.80 | 6.79 | 032 | 42 | 3.232 | 3.229 | $10\bar{8}$ | 8 |
| 6.376 | 6.373 | 110 | 26 | 3.101 | 3.107 | 047 | 4 |
| 6.038 | 6.027 | 040 | 11 | | 3.102 | 154 | |
| 5.977 | 5.972 | $12\bar{1}$ | 18 | 3.077 | 3.079 | $17\bar{1}$ | 8 |
| 5.900 | 5.902 | $11\bar{3}$ | 51 | 2.989 | 2.987 | 171 | 9 |
| | 5.832 | $12\bar{2}$ | | | 2.986 | $24\bar{2}$ | |
| 5.834 | 5.826 | 111 | 12 | | 2.897 | 240 | 5 |
| | 5.827 | 033 | | 2.895 | 2.887 | 172 | |
| 5.619 | 5.615 | 024 | 5 | | 2.900 | $15\bar{7}$ | |
| 5.441 | 5.434 | $12\bar{3}$ | 13 | | 2.901 | $17\bar{4}$ | |
| | 5.444 | $04\bar{2}$ | | 2.872 | 2.875 | $16\bar{6}$ | 5 |
| 5.266 | 5.250 | $11\bar{4}$ | 25 | | 2.872 | 155 | |
| 5.223 | 5.224 | $13\bar{1}$ | 12 | | 2.846 | $23\bar{6}$ | |
| 4.969 | 4.968 | $01\bar{5}$ | 3 | 2.848 | 2.847 | $14\bar{8}$ | 8 |
| 4.530 | 4.532 | $14\bar{1}$ | 7 | | 2.843 | 117 | |
| | 4.542 | 113 | | 2.787 | 2.786 | 127 | 4 |
| 4.366 | 4.370 | $04\bar{4}$ | 11 | | 2.786 | $25\bar{3}$ | |
| | 4.380 | $12\bar{5}$ | | 2.739 | 2.741 | $25\bar{4}$ | 1 |
| 4.310 | 4.318 | 123 | 4 | 2.687 | 2.683 | $15\bar{8}$ | 5 |
| 4.249 | 4.254 | 141 | 7 | | 2.687 | 242 | |
| 4.170 | 4.167 | $01\bar{6}$ | 6 | 2.641 | 2.642 | $17\bar{6}$ | 3 |
| 4.114 | 4.117 | $10\bar{6}$ | 4 | | 2.647 | 204 | |
| 3.993 | 3.992 | 026 | 7 | 2.627 | 2.629 | $18\bar{4}$ | 13 |
| 3.971 | 3.969 | 061 | 8 | | 2.625 | $10\bar{1}0$ | |
| | 3.841 | 124 | | 2.586 | 2.585 | 224 | 14 |
| 3.838 | 3.839 | 054 | 13 | | 2.586 | 147 | |
| | 3.831 | 062 | | 2.552 | 2.552 | 260 | 5 |
| 3.779 | 3.780 | $15\bar{3}$ | 5 | | 2.548 | 252 | |
| 3.742 | 3.743 | 036 | 5 | | 2.505 | $26\bar{5}$ | |
| 3.622 | 3.618 | 134 | 12 | 2.496 | 2.495 | $13\bar{1}0$ | 25 |
| | 3.629 | 063 | | | 2.497 | 077 | |
| | 3.476 | $12\bar{7}$ | | | 2.496 | $19\bar{1}$ | |
| 3.480 | 3.472 | 027 | 7 | 2.482 | 2.484 | 0210 | 7 |
| | 3.469 | $16\bar{1}$ | | | 2.481 | 175 | |
| 3.439 | 3.433 | 160 | 5 | 2.419 | 2.420 | 0310 | 4 |
| | 3.438 | $20\bar{2}$ | | | 2.419 | $27\bar{1}$ | |
| | 3.363 | 144 | | | | | |
| 3.364 | 3.366 | $21\bar{1}$ | 13 | | | | |
| | 3.366 | $15\bar{5}$ | | | | | |

*Note.* Intensities were calculated with Lazy Pulverix program (*17*). $a$ = 6.876(3) Å, $b$ = 24.109(8) Å, $c$ = 26.411(8) Å, $\beta$ = 106.04(3)°.

from a Guinier powder spectrum (Guinier Nonius FR552, $\lambda CuK\bar{\alpha}$ = 1.5418 Å Si as standard) by a least-squares technique taking into account the first 50 reflections (Table III). Low-temperature (140 K) cell parameters refined on the Nonius CAD4

diffractometer from 25 chosen reflections are given in Table II.

## 3. Structure Refinement

The structural calculations were begun first with the tantalum atoms, the positions of which had been determined from a Patterson map. With only these atoms, the reliability factor dropped to about 25%, emphasizing the overwhelming influence of these heavy cations. With the help of Fourier and Fourier difference maps, the other light atoms (S and P) were progressively added. Because they had very high thermal coefficient values, and also due to incompatible atomic distances, the occupancy ratio of nine sulfur atoms had to be divided by two, the structural features of the phase explaining satisfactorily this distribution (see below). The final refinement was conducted with anisotropic factors, except for the sulfur atoms positions with half occupancy, for which, because of their weak contribution and the quality of the recording, the temperature factor was kept isotropic and made identical. A reliability value of $R = 8.9\%$ was finally obtained for the 3104 reflections and 328 variables. A Fourier difference map revealed that the more intense peak corresponded to 3.1(6) $e/Å^3$, the other peak intensities decreasing regularly (the tenth peak for instance is recorded at 2.6 $e/Å^3$). This observation ensured that all the structure atoms had been taken into account in the refinement calculation, the compound composition being $Ta_2P_2S_{11}$, in agreement with the analytical data. In Tables IV and V are gathered the positional and thermal atomic parameters of the structure. Structure factor tables are deposited at ASIS/NAPS.[1]

[1] See NAPS document No. 04485 for 16 pages of supplementary materials from ASIS/NAPS, Microfiche Publications, P.O. Box 3513, Grand Central Station, New York, New York 10163. Remit in advance $4.00 for microfiche copy or for photocopy, $7.75 up to 20 pages plus $.30 for each additional page. All orders must be prepaid.

TABLE IV

POSITIONAL PARAMETERS AND THEIR ESTIMATED STANDARD DEVIATIONS

| | Atom | $x$ | $y$ | $z$ | $B_{eq}$(Å$^2$) |
|---|---|---|---|---|---|
| | $Ta_{1'}$ | 0.6996(4) | 0.5021 (1) | 0.7620 (1) | 3.02(6) |
| | $Ta_1$ | 0.6275(4) | 0.6287 (1) | 0.8027 (1) | 3.56(5) |
| | $Ta_2$ | 0.4665(3) | 0.76920(9) | 0.50930(8) | 1.83(4) |
| | $Ta_{2'}$ | 0.6971(3) | 0.80473(9) | 0.63179(9) | 1.97(5) |
| | $Ta_3$ | 0.0691(4) | 0.0507 (1) | 0.0431 (1) | 2.85(5) |
| I | $S_{1-1}$ | 0.349 (4) | 0.560 (1) | 0.750 (1) | 1.9 (2)* |
| I | $S_{1-2}$ | 0.462 (4) | 0.535 (1) | 0.825 (1) | 1.9* |
| I | $S_{1-3}$ | 0.869 (4) | 0.581 (1) | 0.780 (1) | 1.9* |
| II | $S_{1-1'}$ | 0.967 (4) | 0.571 (1) | 0.826 (1) | 1.9* |
| II | $S_{1-2'}$ | 0.891 (4) | 0.592 (1) | 0.752 (1) | 1.9* |
| II | $S_{1-3'}$ | 0.451 (4) | 0.549 (1) | 0.784 (1) | 1.9* |
| | $S_{1-4}$ | 0.430 (2) | 0.6690 (7) | 0.7168 (6) | 3.0(3) |
| | $S_{1-5}$ | 0.787 (2) | 0.6335 (7) | 0.8989 (6) | 2.9(3) |
| | $S_{1-6}$ | 0.637 (2) | 0.5236 (6) | 0.6658 (5) | 2.4(3) |
| | $S_{1-7}$ | 0.769 (2) | 0.4427 (7) | 0.8416 (6) | 4.4(4) |
| | $S_{1-8}$ | 0.811 (2) | 0.7163 (7) | 0.8013 (6) | 3.1(3) |
| | $S_{1-9}$ | 0.345 (3) | 0.6695 (7) | 0.8326 (7) | 4.2(4) |
| | $S_{1-10}$ | 0.008 (3) | 0.4490 (7) | 0.7562 (6) | 4.5(4) |
| | $S_{1-11}$ | 0.471 (3) | 0.4256 (6) | 0.7208 (6) | 3.3(4) |
| | $S_{2-1}$ | 0.353 (2) | 0.8303 (8) | 0.5750 (6) | 3.5(4) |
| | $S_{2-2}$ | 0.369 (3) | 0.7492 (7) | 0.5936 (7) | 4.2(4) |
| | $S_{2-3}$ | 0.809 (2) | 0.7700 (7) | 0.5613 (6) | 3.1(3) |
| | $S_{2-4}$ | 0.417 (2) | 0.8595 (7) | 0.4631 (6) | 3.9(3) |
| | $S_{2-5}$ | 0.465 (2) | 0.6641 (6) | 0.5132 (6) | 2.8(3) |
| | $S_{2-6}$ | 0.718 (3) | 0.9064 (7) | 0.6272 (8) | 4.0(4) |
| | $S_{2-7}$ | 0.817 (2) | 0.7110 (6) | 0.6731 (6) | 2.9(3) |
| | $S_{2-8}$ | 0.581 (2) | 0.7449 (6) | 0.4310 (5) | 2.3(3) |
| | $S_{2-9}$ | 0.103 (2) | 0.7493 (6) | 0.4620 (6) | 2.7(3) |
| | $S_{2-10}$ | 0.043 (2) | 0.8224 (6) | 0.6892 (6) | 3.0(4) |
| | $S_{2-11}$ | 0.554 (2) | 0.8058 (7) | 0.7098 (5) | 2.9(3) |
| III | $S_{3-1}$ | 0.724 (4) | 0.032 (1) | 0.977 (1) | 2.3(3)* |
| III | $S_{3-2}$ | 0.229 (4) | 0.026 (1) | 0.968 (1) | 2.3* |
| III | $S_{3-3}$ | 0.797 (4) | 1.002 (1) | 1.013 (1) | 2.3* |
| | $S_{3-4}$ | 0.866 (2) | 1.0004 (7) | 0.8717 (6) | 3.3(3) |
| | $S_{3-5}$ | 0.978 (2) | 0.8674 (6) | 1.0175 (6) | 3.1(3) |
| | $S_{3-6}$ | 0.585 (2) | 0.9144 (6) | 0.9105 (6) | 3.1(3) |
| | $S_{3-7}$ | 0.088 (2) | 0.8805 (7) | 0.9108 (6) | 3.1(3) |
| | $P_1$ | 0.345 (3) | 0.2272 (7) | 0.7760 (7) | 3.3(4) |
| | $P_2$ | 1.002 (2) | 0.4051 (6) | 0.8221 (6) | 2.3(3) |
| | $P_3$ | 0.417 (2) | 0.4643 (6) | 0.6513 (6) | 1.9(3) |
| | $P_4$ | 0.474 (2) | 0.1738 (6) | 0.5932 (6) | 2.2(3) |
| | $P_5$ | 0.159 (2) | 0.6669 (6) | 0.4767 (5) | 2.1(3) |

*Note.* Asterisked atoms were refined isotropically. Atoms of groups I, II, and III were refined with an occupancy ratio of $\tau = 0.5$. Anisotropically refined atoms are given in the form of the isotropic equivalent thermal parameter: $\frac{4}{3}*[a^2 * B_{(1,1)} + b^2 * B_{(2,2)} + c^2 B_{(3,3)} + ab(\cos\gamma) * B_{(1,2)} + ac(\cos\beta) * B_{(1,3)} + bc(\cos\alpha) * B_{(2,3)}]$.

## 4. Structure Results and Discussion

### 4.1. Generalities

Before studying the main structural features of $Ta_2P_2S_{11}$, it may be useful to recall briefly some elements of a new approach to structurally describe complex polyhedra

TABLE V

REFINED TEMPERATURE FACTOR EXPRESSIONS—$\beta$'s

| Name | $B_{(1,1)}$ | $B_{(2,2)}$ | $B_{(3,3)}$ | $B_{(1,2)}$ | $B_{(1,3)}$ | $B_{(2,3)}$ |
|---|---|---|---|---|---|---|
| $Ta_{1'}$ | 0.0208(6) | 0.00101(4) | 0.00091(4) | 0.0047(3) | −0.0015(3) | −0.00046(7) |
| $Ta_1$ | 0.0367(6) | 0.00081(4) | 0.00151(4) | −0.0013(3) | 0.0115(2) | −0.00024(7) |
| $Ta_2$ | 0.0116(4) | 0.00068(4) | 0.00084(3) | −0.0005(2) | 0.0031(2) | −0.00034(6) |
| $Ta_{2'}$ | 0.0118(5) | 0.00074(4) | 0.00085(3) | −0.0011(2) | 0.0018(2) | −0.00029(6) |
| $Ta_3$ | 0.0180(6) | 0.00119(4) | 0.00084(4) | 0.0064(3) | −0.0006(2) | −0.00006(7) |
| $S_{1-4}$ | 0.016 (3) | 0.0015 (3) | 0.0010 (2) | −0.002 (2) | 0.002 (1) | −0.0004 (5) |
| $S_{1-5}$ | 0.015 (3) | 0.0017 (3) | 0.0006 (2) | 0.001 (2) | −0.001 (1) | −0.0012 (4) |
| $S_{1-6}$ | 0.022 (3) | 0.0008 (2) | 0.0008 (2) | 0.000 (2) | 0.005 (1) | 0.0005 (4) |
| $S_{1-7}$ | 0.033 (4) | 0.0013 (3) | 0.0025 (3) | 0.008 (2) | 0.015 (1) | 0.0019 (5) |
| $S_{1-8}$ | 0.020 (4) | 0.0010 (3) | 0.0013 (3) | 0.001 (2) | 0.003 (1) | −0.0003 (4) |
| $S_{1-9}$ | 0.026 (4) | 0.0017 (3) | 0.0016 (3) | 0.008 (2) | 0.003 (2) | −0.0015 (5) |
| $S_{1-10}$ | 0.048 (5) | 0.0013 (3) | 0.0012 (2) | 0.008 (2) | 0.009 (2) | 0.0003 (5) |
| $S_{1-11}$ | 0.029 (4) | 0.0007 (3) | 0.0014 (3) | −0.004 (2) | 0.004 (2) | 0.0004 (4) |
| $S_{2-1}$ | 0.014 (3) | 0.0022 (4) | 0.0014 (3) | −0.002 (2) | 0.005 (1) | −0.0014 (5) |
| $S_{2-2}$ | 0.024 (4) | 0.0015 (3) | 0.0020 (3) | −0.004 (2) | 0.002 (1) | −0.0014 (5) |
| $S_{2-3}$ | 0.013 (3) | 0.0015 (3) | 0.0012 (2) | −0.003 (2) | 0.002 (1) | −0.0013 (5) |
| $S_{2-4}$ | 0.037 (4) | 0.0009 (3) | 0.0020 (3) | 0.004 (2) | 0.014 (1) | 0.0008 (4) |
| $S_{2-5}$ | 0.012 (3) | 0.0008 (2) | 0.0015 (3) | −0.004 (2) | −0.001 (2) | −0.0002 (4) |
| $S_{2-6}$ | 0.019 (4) | 0.0009 (3) | 0.0020 (4) | −0.000 (2) | −0.003 (2) | −0.0002 (5) |
| $S_{2-7}$ | 0.021 (3) | 0.0009 (3) | 0.0016 (2) | −0.000 (2) | 0.008 (1) | −0.0001 (4) |
| $S_{2-8}$ | 0.016 (3) | 0.0006 (2) | 0.0013 (2) | −0.001 (1) | 0.006 (1) | −0.0005 (4) |
| $S_{2-9}$ | 0.008 (3) | 0.0015 (3) | 0.0014 (3) | −0.002 (1) | 0.004 (1) | −0.0002 (4) |
| $S_{2-10}$ | 0.018 (4) | 0.0009 (3) | 0.0012 (3) | −0.002 (2) | −0.002 (2) | −0.0002 (4) |
| $S_{2-11}$ | 0.024 (3) | 0.0014 (3) | 0.0009 (2) | −0.001 (2) | 0.007 (1) | −0.0005 (4) |
| $S_{3-4}$ | 0.023 (4) | 0.0016 (3) | 0.0011 (2) | −0.000 (2) | 0.006 (1) | 0.0008 (5) |
| $S_{3-5}$ | 0.019 (3) | 0.0008 (3) | 0.0020 (3) | −0.000 (2) | 0.008 (1) | −0.0003 (4) |
| $S_{3-6}$ | 0.024 (4) | 0.0008 (3) | 0.0013 (3) | 0.000 (2) | 0.003 (2) | 0.0013 (4) |
| $S_{3-7}$ | 0.026 (4) | 0.0014 (3) | 0.0005 (2) | 0.008 (2) | 0.002 (1) | 0.0004 (4) |
| $P_1$ | 0.022 (4) | 0.0010 (3) | 0.0013 (3) | −0.001 (2) | 0.002 (2) | 0.0004 (5) |
| $P_2$ | 0.014 (3) | 0.0009 (3) | 0.0011 (2) | 0.001 (1) | 0.004 (1) | 0.0009 (4) |
| $P_3$ | 0.009 (3) | 0.0008 (3) | 0.0011 (2) | −0.001 (1) | 0.003 (1) | −0.0004 (4) |
| $P_4$ | 0.011 (3) | 0.0008 (3) | 0.0011 (2) | −0.001 (1) | 0.002 (1) | 0.0007 (4) |
| $P_5$ | 0.016 (3) | 0.0011 (3) | 0.0004 (2) | −0.003 (2) | 0.003 (1) | 0.0002 (4) |

*Note.* The form of the anisotropic thermal parameter is $\exp[-(B_{(1,1)} * h^2 + B_{(2,2)} * k^2 + B_{(3,3)} * l^2 + B_{(1,2)} * hk + B_{(1,3)} * hl + B_{(2,3)} * kl)]$.

and their combination, in particular in the *M*–P–S phases, developed recently (*13*).

Because of the occurrence of polyanionic groups, in particular of $(X_2)^{-II}$ pairs ($X$ = S and Se), that are found along with monoatomic ligands, rather complex groups $M(X_i)_mX_n$ (with $i = 2$ in most cases to date) are encountered in the transition metal chalcogenide family and related groups (organometallic and thiophosphate phases, for instance). In order to make it easier to classify and describe these phases, it is possible to see the irregular $M(X_2)_mX_n$ polyhedra as generated from regular polyhedra $MX_i$, i.e., polyhedra without pairs. For instance, let us consider an octahedron $[MX_6]$ (see Fig. 2). The $\alpha$ transformation keeps the same metal coordination number, but introduces a ligand pairing; the $X_2$ pairs are formed from unpaired $X$ corners of the

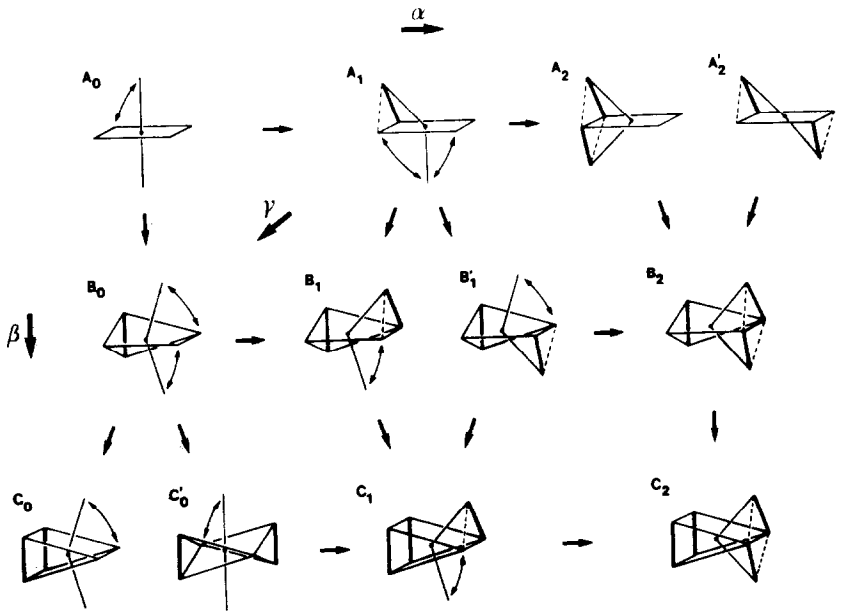


FIG. 2. Generation of complex polyhedra through application to an $A_0$ octahedron of the $\alpha$ and $\beta$ transformation. Also indicated is the deductive $\gamma$-transformation. Thick lines symbolize ligand pairs, and double arrows indicate the ligand atoms involved in pairing, from one configuration to the following one.

original polyhedron. The $\beta$ transformation corresponds to an increase of the coordination number through substitution of a $X$ corner by a $X_2$ group. The $\gamma$ transformation that derives from the two above operations corresponds to the addition of an extra ligand and formation of $X_2$ pairs. All the examples given in Fig. 2 may also correspond to each other by the reverse operations.

So far, VD transition elements have been found to present the coordination $A_0$ and those derived from it, i.e., $B_0$, $B_1$, $C_0$, $C_1$, and $C_2$ (Fig. 1). In the last five configurations, the polyhedra very often share triangular or rectangular faces and they constitute chains or autonomous "bipolyhedra" that allow, in some instances, the occurrence of metal–metal bonding (Fig. 3). The ligands in capping or edge position may be bonded to another identical polyhedron or bipolyhedron, directly (Fig. 4) or through a polyanion (Fig. 5), typically a thiophosphate group in the $M$–P–S family. In more complicated cases, the bipolyhedral units can even share between each other simultaneously an edge, a corner, and a capping ligand (Fig. 6).

The way the bipolyhedral groups are bonded, in particular via their capping or corner ligand, may be related to the crystal space spanning and also to the dimensionality of the phase. For example, let us consider a bipolyhedron constituted by a bicapped biprism $M_2X_{12}$ ($M_2(X_2)_2X_8$) (Fig. 7). With respect to the plane containing the cation ($M$) and the capping ligand ($C$ for capping), the other anions ($E$ and $R$ for edge and rectangle) will be situated either below (subscript D for down) or above (subscript U for up), hence, the labeling given in Fig. 7 (*13*). In certain structures, the connection between polyhedra (directly or through

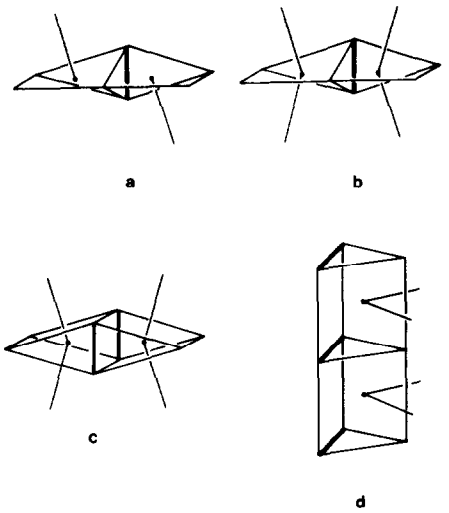


FIG. 3. Examples of obtention of bipolyhedral groups from $A_1$, $B_0$, and $C_0$ units of Fig. 2, by sharing of one triangular face (a and b (with $A_1$ and $B_0$)) and one rectangular face (c (with $C_0$)).

polyanions) is of the *CE/EC* type (Fig. 4), and in the case of four simultaneous such connections, three possibilities exist (Fig. 8). They are $\mathbb{C}_a^4$, $\mathbb{C}_b^4$R, and $\mathbb{C}_b^4$L. The last two configurations are super-labeled R and L (for right and left), since one is the mirror image of the other. It has been shown (*13*)

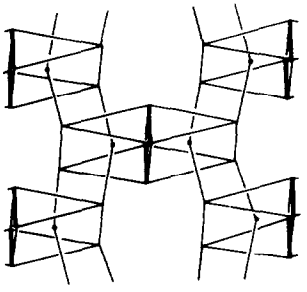

FIG. 4. Direct bonding of the *EC/CE* type through capping and edge sulfur atoms of rectangular face-sharing biprisms as encountered in some transition metal chalcogenides. The structure is that of the $MX_2Y_2$ family ($M$ = VD element; $X$ = S, Se; $Y$ = Cl, Br).

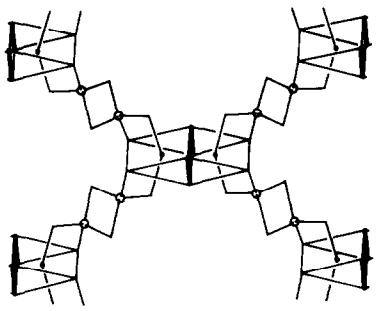

FIG. 5. Indirect bonding of the *EC/CE* type between the same bipolyhedra as in Fig. 4 through ($P_2S_6$) bitetrahedral linking groups. Solid and open circles represent, respectively, the transition metal and phosphorus. The structure is that of 2-D $NbP_2S_8$ (*7*).

that the use of one bonding group rather than the other changes the direction of rotation of the crystal array in some compounds. As an example, let us briefly study the interconnection of the ($M_2X_{12}$) groups through ($PS_4$) units as encountered in $TaPS_6$ (*9*) and $Ta_4P_4S_{29}$ (*10*). The ($Ta_2S_{12}$) bicapped biprisms are bonded to ($PS_4$) tetrahedra as shown in Fig. 9a and the polyhedra then span the crystal space as indicated in Fig. 9b where a large tunnel is hence created. Figure 10 is a schematic of the structure where the type of connection involved at the bipolyhedral site, i.e., $\mathbb{C}_b^4$R, has been given. It one compares Figs. 8 and 9, since the bonds between ($Ta_2S_{12}$) groups are such as the up ($CE_U$) bond of one polyhedron is followed by a down bond ($CE_D$), the ($Ta_2S_{12}$) and ($PS_4$) prisms are rotating coun-

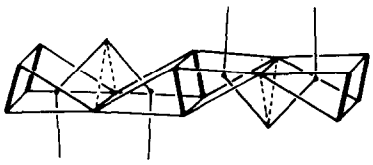

FIG. 6. Complex bonding between $C$ polyhedra involving capping, edge, and rectangular face ligand sharing. This case is encountered for instance in $Nb_3Se_5Cl_7$ (*16*).

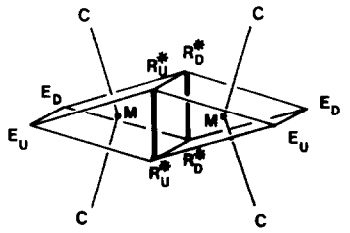


FIG. 7. Labeling of the ligand atoms of a $C_0/C_0$ bipolyhedron with respect to the plane containing the cation ($M$) and capping atoms ($C$).

terclockwise around the large tunnel (U⌒D) to give a right-handed helix. For the adjacent little tunnel, the rotation is clearly opposite (U⌢D), and with respect to that tunnel axis, rotation takes place clockwise (left-handed helix). Obviously change of the sulfur atoms in the interconnections will not change the compound composition, but will imply the direction of rotation (or absence of rotation) of the structure polyhedra. A systematics has been studied for this type of phase (*13*).

### 4.2. $Ta_2P_2S_{11}$ Structure

*4.2.1. General features.* Like the other P–Ta–S phases, the $Ta_2P_2S_{11}$ structure can be described as a gathering of tantalum–sulfur coordination groups interconnected by ($PS_4$) tetrahedral units. The transition metal polyhedra are constituted by the $B_0$ polyhedron of the above classification (Fig. 2). This group is made up of a tantalum cation with a sulfur triangle on one side ($(S_2)^{-II}$–

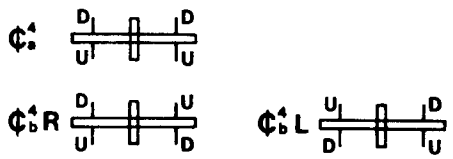


FIG. 8. Schematic representation of a $C_0/C_0$ bipolyhedral cluster (face-sharing prisms) with the four up and down possibilities leading to three types of combinations.

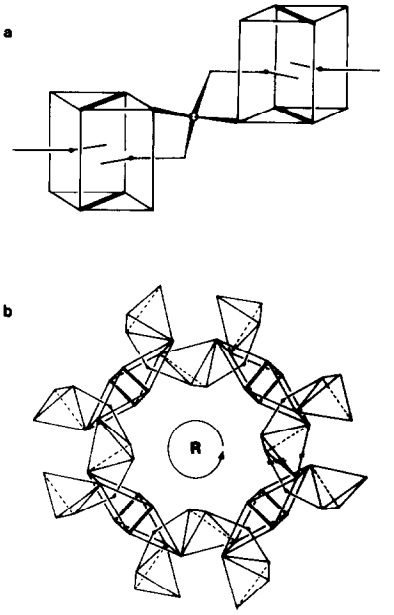


FIG. 9. (a) Indirect combination through a ($PS_4$) linking unit between two biprisms [$Ta_2S_{12}$] in $Ta_4P_4S_{29}$. (b) Rotating arrangement resulting of the [$Ta_2S_{12}$] cluster indirect interconnection (right handed helix).

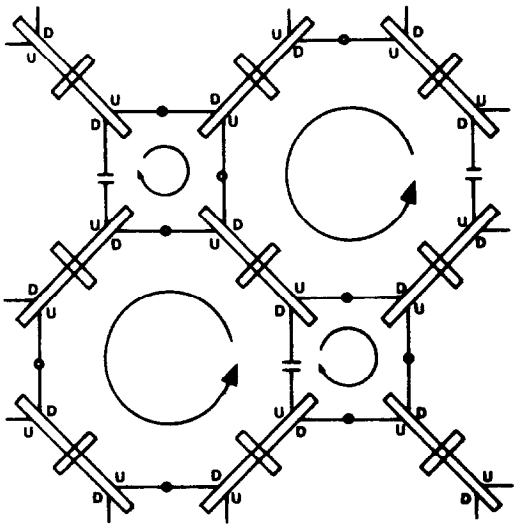


FIG. 10. Schematic representation of the basic tunnel structure revealing the $C_b^4$R connections. Large and small tunnels present, respectively, right- and left-handed polyhedron helix.

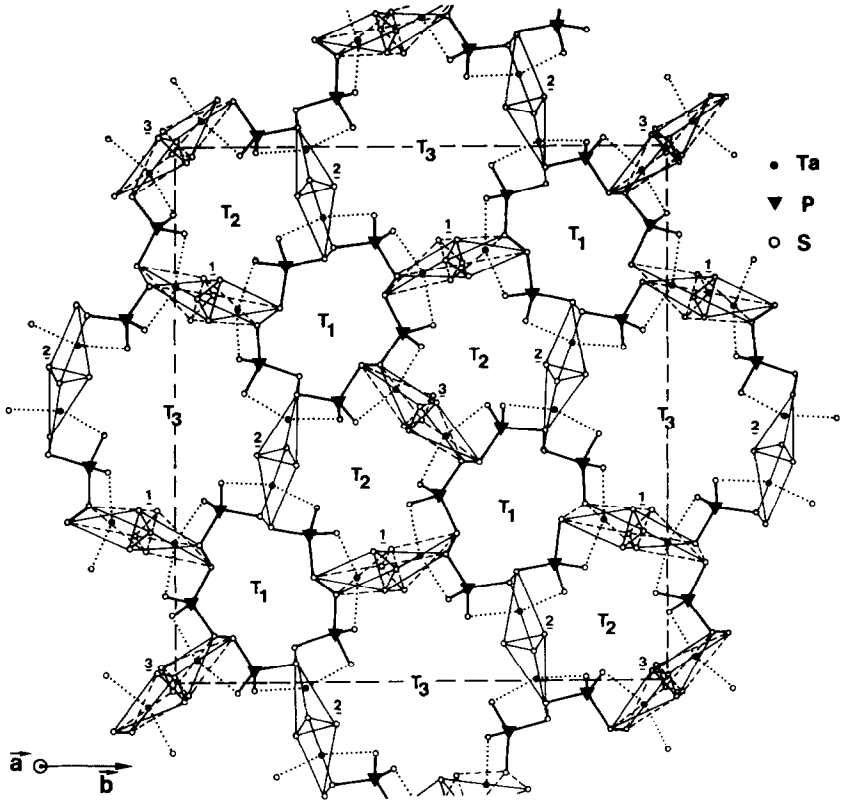


FIG. 11. Projection, along the *a* axis, of $Ta_2P_2S_{11}$ structure that shows the three types of bipolyhedra (labeled 1, 2, and 3) and the three kinds of tunnels ($T_1$, $T_2$, $T_3$). Dotted lines correspond to capping sulfur atoms, and broken lines to the second type of sulfur arrangement resulting from the sulfur disorder on the ($S_3$) triangles of the ($Ta_2S_{11}$) bipolyhedra.

$S^{-II}$) and an edge on the other ($S^{-II}$–$S^{-II}$), with two capping sulfur anions. This induces an heptacoordination of tantalum. Two such units share their triangular face to build a ($Ta_2S_{11}$) bipolyhedron (Fig. 3b). In the structure $Ta_2P_2S_{11}$, there exist five different bipolyhedra, differing only slightly in interatomic angles and distance. Figure 11 is a projection of the structure where three groups of polyhedra (labeled 1, 2, and 3) can be seen. For bipolyhedra 1 and 3 two different orientations of the ($S_3$) triangles have been found, in agreement with the statistical occupation of the corresponding sulfur sites (see Table IV of the atomic position parameters). Clearly, from simple geometrical considerations (see Fig. 3b), both configurations (drawn separately in Fig. 12) are equivalent. In the case of polyhedron 3, this is mandatory as the inversion center of the $P2_1/c$ space group is located at the center of the ($Ta_2S_{11}$) unit. This situation implies very similar energies for the coordination groups. Since the triangular ($S_3$) group is not bonded to any other atomic entities, both configurations take place easily, hence the statistical distribution. Such an atomic arrangement is not unknown and it is of interest to emphasize the case of the organometallic compounds

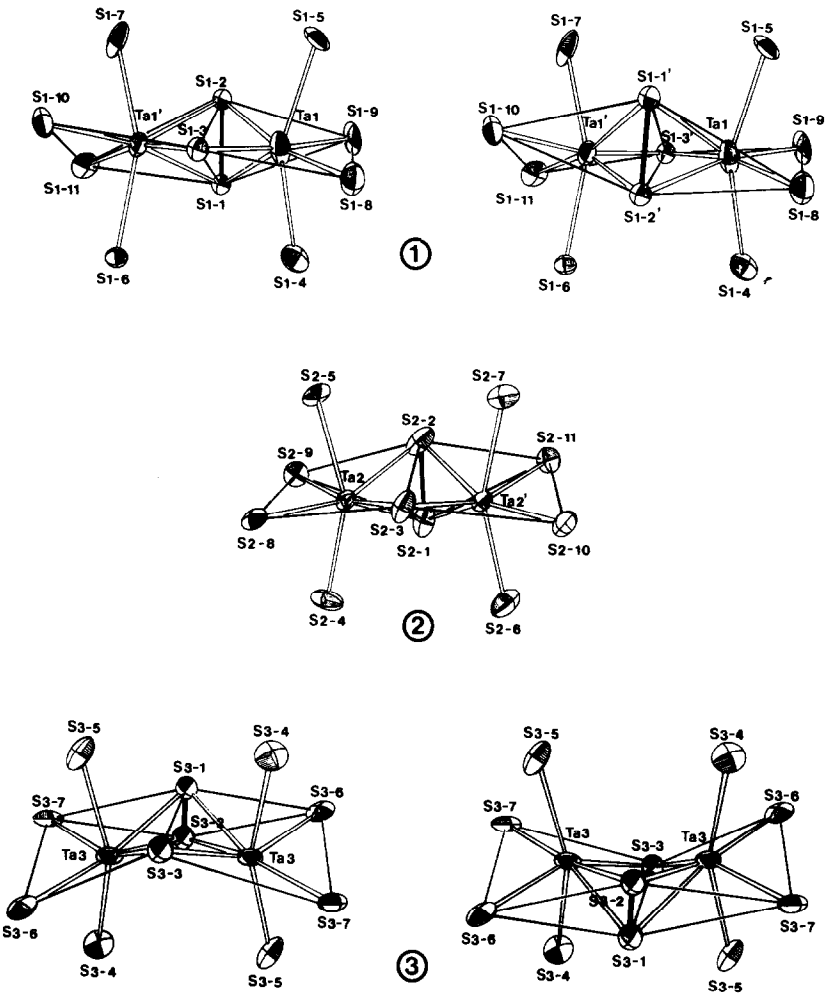


FIG. 12. ORTEP drawings of the different ($Ta_2S_{11}$) bipolyhedra encountered in $Ta_2P_2S_{11}$. (1) and (3) show the two arrangements resulting of the two types of sulfur triangle sets and (2) the other ordered ($Ta_2S_{11}$) biunits.

$Nb_2Cl_4S_3$, $4SC_4H_8$ and $Nb_2Br_4S_3$, $4SC_4H_8$ (*14*). In these phases, the coordination groups are $Nb_2X_4S_7$ ($X$ = Cl, Br), and one finds ($Nb_2S_7X_4$) cages, like the ($Ta_2S_{11}$) ones of ($Ta_2P_2S_{11}$). If the brominated phase presents regular bipolyhedra, the $S_3((S_2)^{-II}$–$S^{-II})$ bridging group of the chlorinated compound is found disordered with two types of positions filled respectively at 66 and 34%. $Ta_2P_2S_{11}$ is a phase where both ordered and disordered ($Ta_2S_{11}$) units are found, the compound gathering the two structural features of the above organometallic phases. In the case of the ($Ta_2S_{11}$) bipolyhedron 1, located in a general position, the occupancy ratio of the two ($S_3$) triangles was set at 50% and not refined, but obviously some departure from that even distribution can take place. The ($Ta_2S_{11}$) groups are bonded to one another through a ($PS_4$) tetrahedron utilizing an edge and capping sulfur atom, in a $\mathbb{C}_a^4$, $\mathbb{C}_b^4R$, and $\mathbb{C}_b^4L$, way. This leaves

three types of tunnels in the structure, two small ($T_1$ and $T_2$) and a large one ($T_3$).

Symbolizing the polyhedra according to Ref. (*13*) and as shown above in the case of the $TaPS_6$ and $Ta_4P_4S_{29}$ structures, one obtains the structure projection of Fig. 13. The $T_1$ tunnels are found to have polyhedra that rotate either clockwise or counterclockwise (right- and left-handed rotation). Around tunnels $T_2$ and $T_3$ no rotation occurs. All the tunnels are found empty, as expected since the frame constituted by the ($Ta_2S_{11}$) and ($PS_4$) polyhedra already corresponds to the analytical composition. Like in the case of the two previous Ta–P–S phases, $Ta_2P_2S_{11}$ is made of two interlocked atomic networks sharing no bonds. To that rather open structure corresponds a fairly low calculated density of 3.06 to be compared to that of more dense phase $TaPS_6$ ($d = 3.25$) and one may wonder why, like it does in the case of $Ta_4P_4S_{29}$ structure, sulfur as a polyatomic group is not filling the void spaces. The answer for $T_1$ and $T_2$ is straightforward: because the diameter of the tunnels is not large enough to accommodate a sulfur helix, but $T_3$ has a size similar to that found in $Ta_4P_4S_{29}$.

A convincing explanation can be put forward to understand that experimental observation. It is to be remembered that in $Ta_4P_4S_{29}$, the $S_{10}$ sulfur helix is right-handed like the surrounding tunnel structure. Polymeric sulfur can only be obtained under high pressure (*15*) and occurrence of such a chain in a solid state phase like $Ta_4P_4S_{29}$ obtained under low pressure must then be ascribed to a sort of steric pressure. This is probably possible for rotating tunnel structures only. Since there are only van der

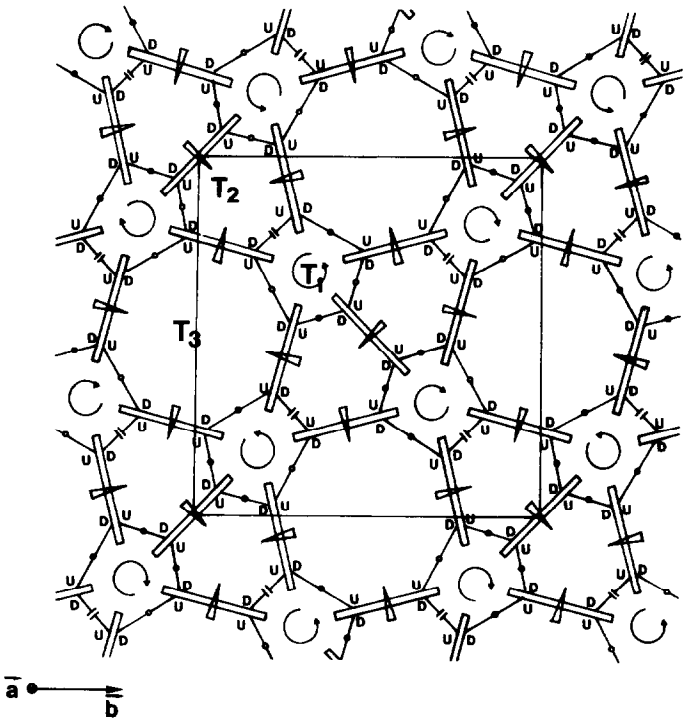


FIG. 13. Schematic representation of $Ta_2P_2S_{11}$ structure projected (as in Fig. 11) along the *a* axis, using the systematization and labeling developed in Ref. (*13*).

Waals distances between the helix atoms and the basic tunnel structure (BTS), the sulfur chain develops in an orderly way that can only be explained if one assumes that the empty sites left by the BTS are commensurate with the chain and lock it. The atomic groups constituting the $T_3$ tunnels do not rotate and the $Ta_2P_2S_{11}$ structural frame cannot exert any steric pressure; hence, the void observed. The structure of selenium-substituted $TaPS_6Se$ seems to support this analysis (*11*).

*4.2.2. Structure analysis.* Tables IV and V give the positional parameters and the temperature factor expressions, while Table VI presents the main interatomic angles and distances found in $Ta_2P_2S_{11}$. The hepta-coordinated tantalum atoms yield a Ta–S mean distance of 2.494 Å, compared to 2.539 and 2.536 Å, respectively, in $Ta_4P_4S_{29}$ (*10*) and $TaPS_6$ (*9*). Still, as can be seen in Table VI, some dispersion of the distances is shown. This is probably to be attributed to the poor crystal quality, as explained in the experimental section. However, some bonds length differences are expected because of the nature of the ($S_3$) triangles ($(S_2)^{-II}$–$S^{-II}$) shared by two tantalum atoms. For example, in a compound such as

TABLE VI

MAIN INTERATOMIC DISTANCES (IN Å) AND ANGLES (IN DEGREES) IN $Ta_2P_2S_{11}$ (ESD IN PARENTHESES)

| | | | |
|---|---|---|---|
| [$Ta_2S_{11}$] bipolyhedron 1 (with disordered $S_3$ triangle) | | | |
| $Ta_{1'}$–$S_{1-1}$ | 2.719(16) | $Ta_1$–$S_{1-1}$ | 2.618(16) |
| $S_{1-2}$ | 2.736(16) | $S_{1-2}$ | 2.658(16) |
| $S_{1-3}$ | 2.195(17) | $S_{1-3}$ | 2.233(17) |
| $S_{1-1'}$ | 2.688(16) | $S_{1-1'}$ | 2.638(16) |
| $S_{1-2'}$ | 2.589(17) | $S_{1-2'}$ | 2.667(17) |
| $S_{1-3'}$ | 2.252(16) | $S_{1-3'}$ | 2.242(16) |
| $S_{1-6}$ | 2.507(9) | $S_{1-4}$ | 2.494(10) |
| $S_{1-7}$ | 2.474(10) | $S_{1-5}$ | 2.473(9) |
| $S_{1-10}$ | 2.504(11) | $S_{1-8}$ | 2.456(10) |
| $S_{1-11}$ | 2.468(10) | $S_{1-9}$ | 2.476(10) |
| [$Ta_2S_{11}$] bipolyhedron 2 | | [$Ta_2S_{11}$] bipolyhedron 3 (with disordered ($S_3$) triangle) | |
| $Ta_2$– $S_{2-1}$ | 2.547(10) | $Ta_3$–$S_{3-1}$ | 2.571(17) |
| $S_{2-2}$ | 2.532(12) | $S_{3-1}$ | 2.571(17) |
| $S_{2-3}$ | 2.369(9) | $S_{3-2}$ | 2.566(18) |
| $S_{2-4}$ | 2.467(10) | $S_{3-2}$ | 2.707(19) |
| $S_{2-5}$ | 2.530(9) | $S_{3-3}$ | 2.163(18) |
| $S_{2-8}$ | 2.465(8) | $S_{3-3}$ | 2.321(18) |
| $S_{2-9}$ | 2.506(9) | $S_{3-4}$ | 2.491(9) |
| $Ta_{2'}$–$S_{2-1}$ | 2.495(11) | $S_{3-5}$ | 2.502(10) |
| $S_{2-2}$ | 2.569(10) | $S_{3-6}$ | 2.493(10) |
| $S_{2-3}$ | 2.347(9) | $S_{3-7}$ | 2.463(9) |
| $S_{2-6}$ | 2.455(10) | | |
| $S_{2-7}$ | 2.541(9) | | |
| $S_{2-10}$ | 2.475(9) | Mean Ta–S distance 2.494 | |
| $S_{2-11}$ | 2.506(8) | | |

TABLE VI—*Continued*

| | | | |
|---|---|---|---|
| ($PS_4$) tetrahedra | | | |
| $P_1$–$S_{1-4}$ | 2.051(14) | $S_{1-4}$ –$P_1$–$S_{1-8}$ | 100.3(6) |
| $S_{1-8}$ | 2.040(15) | $S_{1-4}$ –$P_1$–$S_{2-7}$ | 110.0(6) |
| $S_{2-7}$ | 1.993(13) | $S_{1-4}$ –$P_1$–$S_{2-11}$ | 114.4(6) |
| $S_{2-11}$ | 2.012(14) | $S_{1-8}$ –$P_1$–$S_{2-7}$ | 114.3(6) |
| | | $S_{1-8}$ –$P_1$–$S_{2-11}$ | 111.5(6) |
| | | $S_{2-7}$ –$P_1$–$S_{2-11}$ | 106.5(6) |
| $P_2$–$S_{1-7}$ | 2.018(12) | $S_{1-7}$ –$P_2$–$S_{1-10}$ | 100.6(6) |
| $S_{1-10}$ | 2.041(14) | $S_{1-7}$ –$P_2$–$S_{2-6}$ | 119.9(7) |
| $S_{2-6}$ | 2.012(14) | $S_{1-7}$ –$P_2$–$S_{2-10}$ | 112.2(6) |
| $S_{2-10}$ | 2.025(13) | $S_{1-10}$–$P_2$–$S_{2-6}$ | 108.8(6) |
| | | $S_{1-10}$–$P_2$–$S_{2-10}$ | 114.9(6) |
| | | $S_{2-6}$–$P_2$–$S_{2-10}$ | 101.1(6) |
| $P_3$–$S_{1-6}$ | 2.031(12) | $S_{1-6}$ –$P_3$–$S_{1-11}$ | 102.4(5) |
| $S_{1-11}$ | 1.998(13) | $S_{1-6}$ –$P_3$–$S_{3-4}$ | 110.4(5) |
| $S_{3-4}$ | 2.061(13) | $S_{1-6}$ –$P_3$–$S_{3-6}$ | 114.4(5) |
| $S_{3-6}$ | 2.020(12) | $S_{1-11}$–$P_3$–$S_{3-4}$ | 112.9(6) |
| | | $S_{1-11}$–$P_3$–$S_{3-6}$ | 114.9(6) |
| | | $S_{3-4}$ –$P_3$–$S_{3-6}$ | 102.3(5) |
| $P_4$–$S_{1-5}$ | 2.089(13) | $S_{1-5}$ –$P_4$–$S_{1-9}$ | 101.2(5) |
| $S_{1-9}$ | 2.013(14) | $S_{1-5}$ –$P_4$–$S_{2-4}$ | 112.9(6) |
| $S_{2-4}$ | 1.999(13) | $S_{1-5}$ –$P_4$–$S_{2-8}$ | 112.6(5) |
| $S_{2-8}$ | 2.060(12) | $S_{1-9}$ –$P_4$–$S_{2-4}$ | 116.4(7) |
| | | $S_{1-9}$ –$P_4$–$S_{2-8}$ | 111.2(6) |
| | | $S_{2-4}$ –$P_4$–$S_{2-8}$ | 102.9(5) |
| $P_5$–$S_{2-5}$ | 2.048(12) | $S_{2-5}$ –$P_5$–$S_{2-9}$ | 103.8(5) |
| $S_{2-9}$ | 2.036(13) | $S_{2-5}$ –$P_5$–$S_{3-5}$ | 115.5(6) |
| $S_{3-5}$ | 2.025(12) | $S_{2-5}$ –$P_5$–$S_{3-7}$ | 111.2(6) |
| $S_{3-7}$ | 2.023(12) | $S_{2-9}$ –$P_5$–$S_{3-5}$ | 112.7(6) |
| | | $S_{2-9}$ –$P_5$–$S_{3-7}$ | 113.4(6) |
| | | $S_{3-5}$ –$P_5$–$S_{3-7}$ | 100.6(5) |
| mean P–S distance 2.030 | | mean S–P–S angle 109.5 | |
| [$S_2$] pairs of the ($S_3$) triangle | | | |
| $S_{1-1}$ –$S_{1-2}$ | 2.017(23) | | |
| $S_{1-1'}$–$S_{1-2'}$ | 1.951(24) | | |
| $S_{2-1}$ –$S_{2-2}$ | 2.005(16) | | |
| $S_{3-1}$ –$S_{3-2}$ | 1.974(25) | | |

$Nb_2Br_4S_3$ (*14*), the structure of which was refined to $R = 0.061$, the niobium atoms are closer to the monoatomic anion ($d_{Nb-S} \simeq 2.33$ Å) than to the $(S_2)^{-II}$ pair ($d_{Nb-S} \simeq 2.49$ Å). The same difference is observed in $Ta_2P_2S_{11}$ in the case of the bipolyhedron with full occupancy of the sulfur in triangular position (group 2) with a mean Ta–S distance of 2.36 and 2.54 Å, respectively with $S^{-II}$ and $(S_2)^{-II}$. The phenomenon is amplified in the case of disordered polyhedra 1 and 2 for which one calculates strong dispersion ($d_{Ta-S} = 2.16$ Å and $d_{Ta-S} = 2.72$ Å). This is certainly to be also attributed to the small contribution of the half-filled sulfur positions as opposed to heavy tantalum atoms.

By contrast, the dispersion of the P–S bond lengths is small (mean $d_{P-S} = 2.03 \pm 0.02$ Å). The same cannot be said about the S–S distances of the $S_2$ pairs and the difficulties encountered in obtaining proper values for these bonds in the room temperature structure determination data have been pointed out earlier. Two of the distances ($S_{1-1'}$–$S_{1-2'}$ and $S_{3-1}$–$S_{3-2}$) calculated at 1.95(2) and 1.97(2) Å are too short for such a diatomic anion. This is, in part, to be related to the small diffraction weight of the corresponding atoms sites only filled at 50%. However, taking into account the estimated standard deviations, regular distances can be reached.

Considering the two types of anions of the cell ($S_2^{-II}$ and $S^{-II}$), an oxidation state of V for the tantalum atom as inferred from the Ta–S distances, and assuming the same oxidation state of five for phosphorus atoms as always found for tetrahedral ($PS_4$) groups, one finds the charge balance $Ta_2^{V}P_2^{V}(S_2)^{-II}S_9^{-II}$. This type of formulation is quite typical of the *M*–P–S phases (*M* = V, Nb, and Ta), and considering the structural features and interatomic distances, semiconducting and diamagnetic (or insulator) properties are expected.

The last observation to be done concerns the values of the equivalent thermal factors that, although quite lower than for the room temperature structure, are all rather high, especially if compared to that of related phases. This can be tentatively linked to the small compacity of the structure, inducing more freedom for the motion of the atoms. More important motions had been pointed out for less strongly bonded atoms in the case of $Ta_4P_4S_{29}$, for instance (*10*). The high thermal factors can be linked to the occurrence of sulfur disorder at the bipolyhedral sites 1 and 3. For these groups, $E_{eq}$ of tantalum is rather high ($\simeq 3.2$ Å$^2$), the thermal motion incorporating the local induced distortion. In effect, for group 2 with an ordered ($S_3$) face, a reasonable value of $B_{eq} = 1.9$ Å$^2$ is calculated for the cations.

## 5. Conclusion

Combination of tantalum, phosphorus, and sulfur seems to lead systematically to tunnel structures made of interlocked systems themselves built from complex polyhedral interconnections. In $Ta_2P_2S_{11}$, these polyhedra are constituted by ($PS_4$) and ($Ta_2S_{11}$) coordination groups, the former being a tetrahedron and the latter a more original bipolyhedron in which tantalum exerts an heptacoordination. The largest tunnel has a size suitable for sulfur chain insertion and is unexpectedly empty. This phenomenon can be related to the particular arrangement of the ($PS_4$) and ($Ta_2S_{11}$) polyhedra which, contrary to other materials, do not form in their interconnection, rotating helix-like system around the main tunnel axis.

The complex charge balance of the compound (expected to be diamagnetic and semiconducting), written $Ta_2^{V}P_2^{V}(S_2)^{-II}S_9^{-II}$, is a familiar feature of the thiophosphates of VD transition metal. For example, $TaPS_6$ and $Ta_4P_4S_{29}$ were found to correspond respectively to $Ta^{V}P^{V}(S_2)^{-II}S_4^{-II}$ and $Ta_4^{V}P_4^{V}(S_2)_4^{-II}S_{16}^{-II}S_5^{0}$. Following recent sys-

tematic considerations in polyhedra (*13*) and their potential combinations, the possibility exists that several other phases with low density may occur. This would deserve further exploration of the *M*–P–S systems.

## Acknowledgments

The authors thank Dr. M. Sergent for his help in the low temperature crystal data recording and fruitful advice. They also thank the NATO postdoctoral program and the CNRS for providing financial support for this work.

## References

1. G. Ouvrard, R. Freour, R. Brec, and J. Rouxel, *Mater. Res. Bull.* **20,** 1053 (1985).
2. R. Brec, R. Freour, G. Ouvrard, J. L. Soubeyroux, and J. Rouxel, *Mater. Res. Bull.* **18,** 689 (1983).
3. R. Brec, G. Ouvrard, M. Evain, P. Grenouilleau, and J. Rouxel, *J. Solid State Chem.* **47,** 174 (1983).
4. M. Evain, R. Brec, G. Ouvrard, and J. Rouxel, *J. Solid State Chem.* **56,** 12 (1985).
5. R. Brec, P. Grenouilleau, M. Evain, and J. Rouxel, *Rev. Chim. Miner.* **20,** 295 (1983).
6. R. Brec, M. Evain, P. Grenouilleau, and J. Rouxel, *Rev. Chim. Miner.* **20,** 283 (1983).
7. P. Grenouilleau, R. Brec, M. Evain, and J. Rouxel, *Rev. Chim. Miner.* **20,** 628 (1983).
8. M. Evain, R. Brec, G. Ouvrard, and J. Rouxel, *Mater. Res. Bull.* **18,** 41 (1984).
9. S. Fiechter, W. F. Kuhs, and R. Nitsche, *Acta Crystallogr. Sect. B* **36,** 2217 (1980).
10. M. Evain, M. Queignec, R. Brec, and J. Rouxel, *J. Solid State Chem.* **56,** 148 (1985).
11. M. Evain, M. Queignec, C. Sourisseau, and R. Brec, *J. Solid State Chem.*, in press.
12. B. Frenz, "Enraf–Nonius, Structure Determination Package," Delft, Univ. Press, Delft (1983).
13. M. Evain, Submitted for publication.
14. M. G. B. Drew, D. A. Rice, and D. M. Williams, *J. Chem. Soc. Dalton Trans.*, 2251 (1983).
15. M. D. Lind and S. Geller, *J. Chem. Phys.* **51,** 348 (1959).
16. J. Rijnsdorp and F. Jellinek, *J. Solid State Chem.* **28,** 149 (1979).
17. R. Yvon, W. Jeitschko, and E. Parthe, *J. Appl. Crystallogr.* **10,** 73 (1977).